*Journal of Microscopy, Vol. 234, Pt 1 2009, pp. 95–102*
*Received 3 June 2008; accepted 26 November 2008*

# High-resolution X-ray tomography of the human inner ear: synchrotron radiation-based study of nerve fibre bundles, membranes and ganglion cells

A. LAREIDA*,†, F. BECKMANN‡, A. SCHROTT-FISCHER§, R. GLUECKERT§, W. FREYSINGER§ & B. MÜLLER*†
**Biomaterials Science Center, University of Basel, c/o University Hospital, 4031 Basel, Switzerland*
*†Computer Vision Laboratory, ETH Zürich, Sternwartstrasse 7, 8092 Zürich, Switzerland*
*‡Institute for Materials Research, GKSS-Research Center, Max-Planck-Strasse 1, 21502 Geesthacht, Germany*
*§Department of Otorhinolaryngology, Innsbruck Medical University, Anichstrasse 35, 6020 Innsbruck, Austria*

**Key words.** Cochlea, ganglion cell counting, osmium stain, synchrotron radiation, X-ray micro tomography.

**Summary**

The combination of osmium tetroxide staining and high-resolution tomographic imaging using monochromatic X rays allows visualizing cellular structures of the human inner ear, that is, the organ of Corti, the stria vascularis and further soft tissues of the membranous labyrinth, in three-dimensional space with isotropic micrometre resolution. This approach permits to follow the course of nerve fibre bundles in a major part of the specimen and reveals the detailed three-dimensional arrangement of individual ganglion cells with distinct nuclei by means of X-ray tomography for the first time. The non-destructive neuron cell counting in a selected volume of 125 μm × 800 μm × 600 μm = 0.06 $mm^3$ gives rise to the estimate that 2000 ganglion cells are present along 1 mm organ of Corti.

## Introduction

The hearing organ belongs to the most complex anatomical structures in the human body combining different types of delicate hard and soft tissues (Kiernan, 2006). Since already minor morphological deviations may result in crucial hearing deficiencies as hypothesized (Kiernan, 2006), the detailed knowledge of the human inner ear morphology is essential to achieve a better understanding of the inner ear pathologies (malformations), to improve the design and the insertion procedures of adapted cochlear implants as well as the treatment of hearing diseases. Consequently, imaging down to cellular or even sub-cellular level, which has not been achieved by clinical imaging modalities nor any kind of magnetic resonance imaging (Vogel, 1999), is mandatory for the visualization of the essential soft tissue parts of the inner ear: membranes, nerve fibre bundles, and ganglion cells. Micro computed tomography (μCT) provides the necessary spatial resolution (Plouraboué *et al.*, 2004). The morphology of the inner ear, however, is difficult to access because the functional soft tissues are surrounded by hardest human tissue, the petrous bone, which exhibits strong X-ray absorption (Goldfeld *et al.*, 2005). In order to attain the contrast needed for the identification of cellular features or even individual cells, one has to incorporate highly absorbing species such as osmium tetroxide to increase the X-ray absorption of the soft tissues and to reach absorption levels that are closer to the surrounding bone. Osmium tetroxide, routinely applied to prepare tissues for electron microscopy, reacts with the unsaturated fatty acids and therefore essentially increases the X-ray absorption of cell membranes. Most of the petrous bone should be removed from the specimen to advance the spatial resolution of the tomographic data.

So far, the detailed morphological studies of the delicate microstructures such as sensory membranes, ganglion cells and nerve fibre bundles as parts of the inner ear exclusively rely on histological sectioning. By the sectioning, however, the soft tissues are mechanically deformed near blade that often leads to damages of the thin membranes but at least to their relaxation to straight linear objects. This means that the complex anatomical structures of the inner ear can notably change their morphology, so that tissue shape and thickness can only be estimated (Li *et al.*, 2006). Our approach should allow uncovering the different delicate microstructures in

Correspondence to: Prof. Dr. Bert Müller. Tel: +41 61 265 9660; Fax: +41 61 265 9699; e-mail: bert.mueller@unibas.ch

the three-dimensional (3D) space with isotropic sub-cellular resolution non-destructively and serve as complementary method to the classical histology of the inner ear.

The purpose of this study was to reveal osmium-stained cellular structures, in particular selected delicate membranous microstructures of the sensory organ, nerve fibre bundles and individual ganglion cells of the human cochlea, taking advantage of synchrotron radiation-based micro computed tomography (SRμCT).

## Materials and methods

### *Cochlea preparation*

The human cochlea of a man, 50 years old with normal hearing, was removed 3–5 h after death. The surrounding petrous bone was cut off. Oval and round windows were opened to ensure fast penetration of the fixative into the labyrinth. The fixation was carried out in Karnowsky's formaldehyde solution consisting of 4% paraformaldehyde with 0.1% glutaraldehyde in 0.1 M cacodylate buffer (pH 7.4) at a temperature of 4°C for 1 h. Previous SRμCT-experiments (Vogel, 1999) have shown that freshly explanted cochleae do not exhibit a sufficiently high X-ray absorption contrast to visualize the tiny features of the soft-tissue structures of the organ of Corti. To improve the contrast of the soft tissue with respect to the surrounding, the specimen was post-fixed using 1% $OsO_4$ in 0.05 M cacodylate buffer (pH 7.4) at a temperature of 4°C during 1 h. Finally, the cochlea was dehydrated in a series of graded ethanol and embedded in Spurr's low viscosity epoxy resin, according to the block surface technique for human inner ears (Spoendlin & Schrott, 1988, 1989).

### *Synchrotron radiation-based micro computed tomography*

The SRμCT-measurements at HASYLAB at DESY (Hamburg, Germany) were performed using synchrotron radiation generated in the storage ring DORIS III. The standard set-up for absorption contrast μCT, operated by the GKSS-Research Center, was installed at the beamline BW 2 (Beckmann, 2001). The highly intense, collimated X-ray beam was monochromatized by means of a fixed-exit double crystal monochromator to the photon energy of 10.8 keV with the bandwidth of 0.01%.

The tomography set-up, installed 40 m from the radiation source, consisted of the sample manipulator and the two-dimensional detection unit. The sample manipulator was not only used for the precise sample rotation but also for sample translation to record the photon distribution within the X-ray beam for normalization. The X-ray detection unit consisted of the luminescent screen (500-μm-thick $CdWO_4$ single crystal), the optical lens (Nikkor 35 mm focal length, Nikon Inc., Tokyo, Japan), and the CCD-camera (KX2, Apogee Instruments Inc., Roseville, CA, USA, 14-bit digitization at 1.25 MHz, 1536 × 1024 pixels, each 9 × 9 $\mu m^2$). The luminescent screen converted the incident X rays into visible light, projected with the magnification of 4.3 onto the CCD chip (Müller *et al.*, 2007). A total of 721 projections were recorded for equidistant specimen rotation steps between 0 and 180°.

The spatial resolution of the entire tomography system was experimentally characterized using the 10% value of the modulation transfer function (Müller *et al.*, 2001) found to be 4.3 μm at the photon energy of 10.8 keV and the pixel size of 2.1 μm, which corresponds to a field of view of 3.3 mm × 2.2 mm.

The SRμCT-measurements at the Swiss Light Source (SLS, Paul Scherrer-Institut, Villigen, Switzerland) were carried out at the beamline Tomcat (Stampanoni *et al.*, 2006).

The multi-layer monochromator combined with the 50-μm Al filter provided 2–3% photon energy bandwidth. With the PCO2000 detector (PCO AG, Kelheim, Germany, 2048 × 2048 pixels) 1501 projections between 0 and 180° were recorded.

The data were acquired applying a photon energy of 12 keV with an optical magnification of 4 and an effective pixel size of 1.75 μm and a field of view of 3.6 mm × 3.6 mm.

Since the X rays of the synchrotron radiation sources are almost parallel, the tomograms have been reconstructed slicewise using the filtered back-projection algorithm (Kak & Slaney, 1988).

### *Data processing*

For the 3D visualization of the inner ear, the data were binned by the factors 2, 3 and 4. Binning decreases the spatial resolution but leads to higher-density resolution or contrast (Thurner *et al.*, 2004). Therefore, semi-automatic, intensity-based segmentation usually becomes easier for higher binning factors. To segment the features of interest, the software VG Studio Max 1.2 (Volume Graphics, Heidelberg, Germany) was applied.

## Results

Figure 1 shows a selected virtual cut of the sensory organ in the apical turn of the human cochlea that has been extracted from the tomogram measured at the beamline BW2. In order to reduce the noise level and to increase the contrast, the image has been binned by the factor of 2 resulting in the pixel size of 4.2 μm × 4.2 μm. The highest local absorption level of about 23.5 $cm^{-1}$ has been found for the otic capsule, which surrounds the cochlea and the modiolus containing the auditory nerve. It is visible at the bottom right edge of the slice in Fig. 1. In the lower left part of the slice, one recognizes the delicate bony layers of the osseous spiral lamina (OSL) that also exhibit strong X-ray absorption and span to the belly-shaped organ of Corti in the apical turn. Another highly absorbing structure is the stria vascularis. It consists

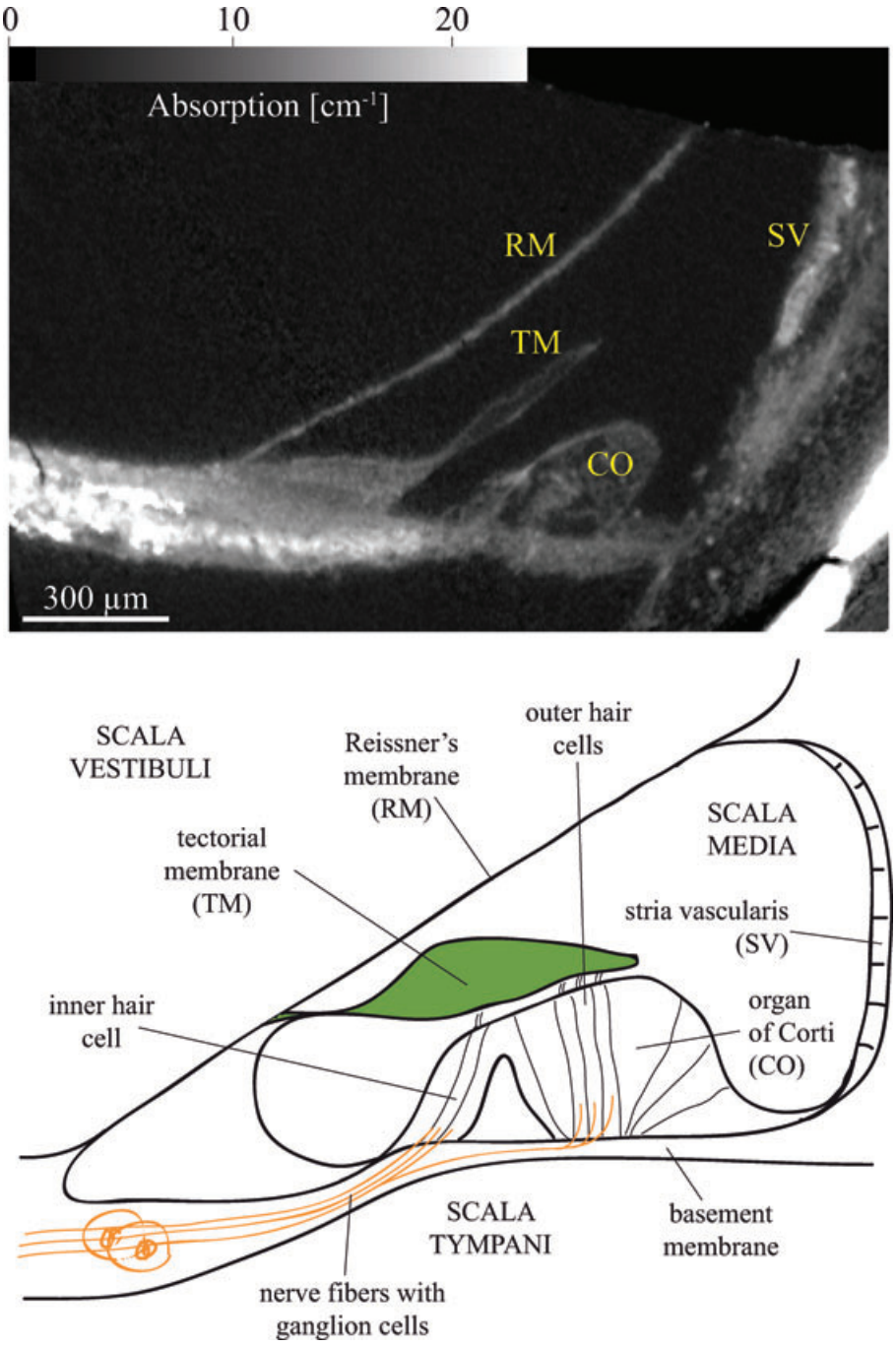


**Fig. 1.** In the selected tomographic slice of the apical turn of the inner ear, the Reissner's membrane (RM), the tectorial membrane (TM), the organ of Corti (CO) and the stria vascularis (SV) are clearly recognized. The scheme helps identifying the morphological features within the representative tomography slice of the human cochlea.

of three different cell layers and plays an important role in ion homeostasis of the endolymphe. The absorption level, here, is inhomogeneously distributed and ranges from about $6.4\,\mathrm{cm}^{-1}$ to $11.5\,\mathrm{cm}^{-1}$. Moderate absorption levels are present in the myelin sheaths around the nerve fibres because of the preferred osmium accumulation (Glauert, 1980). These nerve fibres are known to connect the spiral ganglion neurons in the cochlea with the sensory cells. The nerve fibres are surrounded by the myelin sheaths in the OSL but loose the sheaths at the sensory organ. Hence, they do not silhouette against the organ of Corti.

The prominent morphological features in the slice of Fig. 1 are the Reissner's, tectorial and basement membranes as well as the organ of Corti. The basilar and the Reissner's membranes

 

divide the helically coiled tube of the cochlea into its two compartments. The space between the membranes is known as the cochlear part of the endolymphatic space surrounded by perilymphatic fluid spaces. The Reissner's membrane is composed of epithelial and mesothelial cells forming the double layer attaching to the perilymphatic space. Although the individual cells could not be segmented in the tomography data, the average thickness of the membrane was determined to $(10 \pm 2)$ μm and thus supports the histological findings (de Fraissinette *et al.*, 1993). The presence of nuclei and perikarya causes the observed modulations in the membrane thickness on micrometre scale.

The organ of Corti consists of different types of cells, namely, sensory or hair cells and supporting cells that might be perceived in the slice of Fig. 1. The classification of individual cells, however, has been impossible because of the unspecific osmium stain.

The scheme in Fig. 1 illustrates the morphological features of the tomography data. The three membranes mentioned earlier and the organ of Corti attaching to the basilar membrane form helical structures along the two and a half turns of the human cochlea. A part of this helix is shown in the 3D representations of Fig. 2. Although only a part of the helix has been visualized, the sequence of images may elucidate the spiral shape of the Reissner's and tectorial membranes and the rather complex morphology of the organ of Corti. The images indicate that any virtual cut of the tomography data always provides curve-shaped membranes and does not yield to straight features as presented in schematic illustrations and histological sections.

The nerve fibre bundles also exhibit a complex 3D morphology, which is difficult to extract from histological slices. Figure 3 shows tomography data of the sensory organ of the basal turn with nerve fibre bundles, measured at the

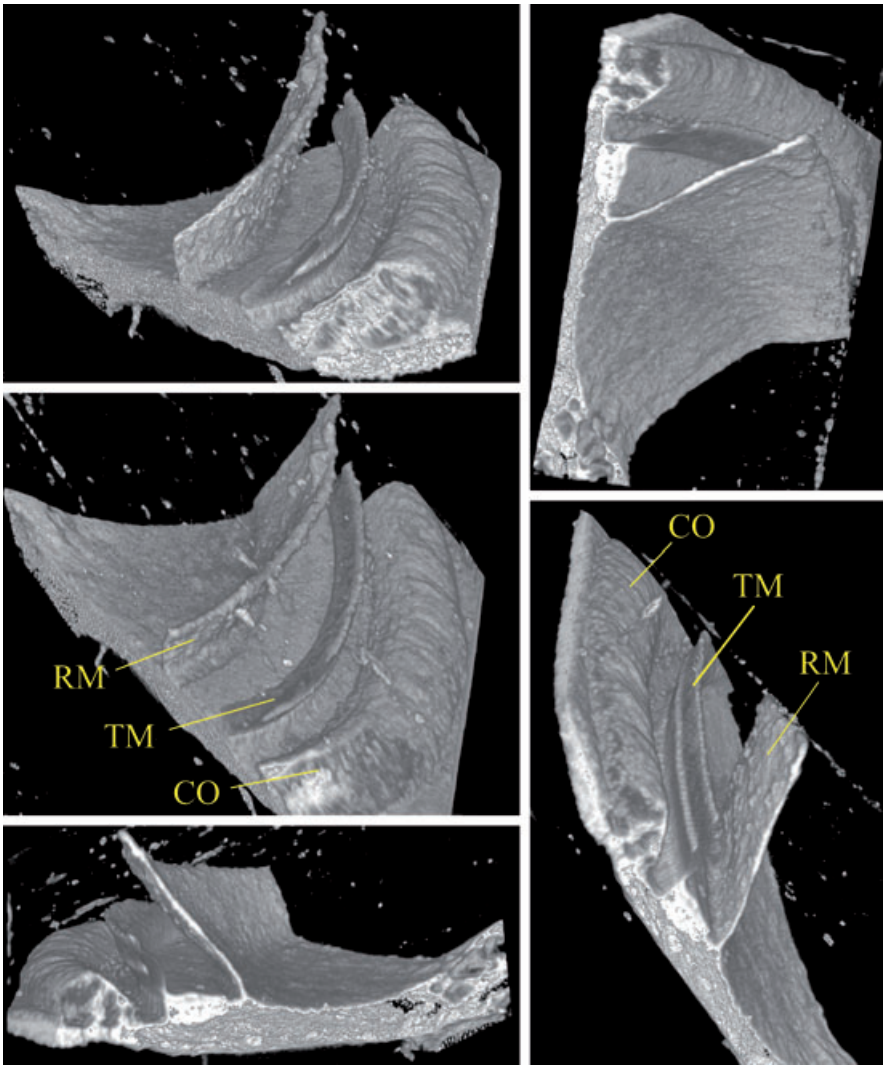


**Fig. 2.** The 3D representations demonstrate the helical shape of the Reissner's membrane (RM), of the tectorial membrane (TM) and of the organ of Corti (CO), which do not exhibit straight sections. A virtual cut always contains curved parts of the selected membrane.

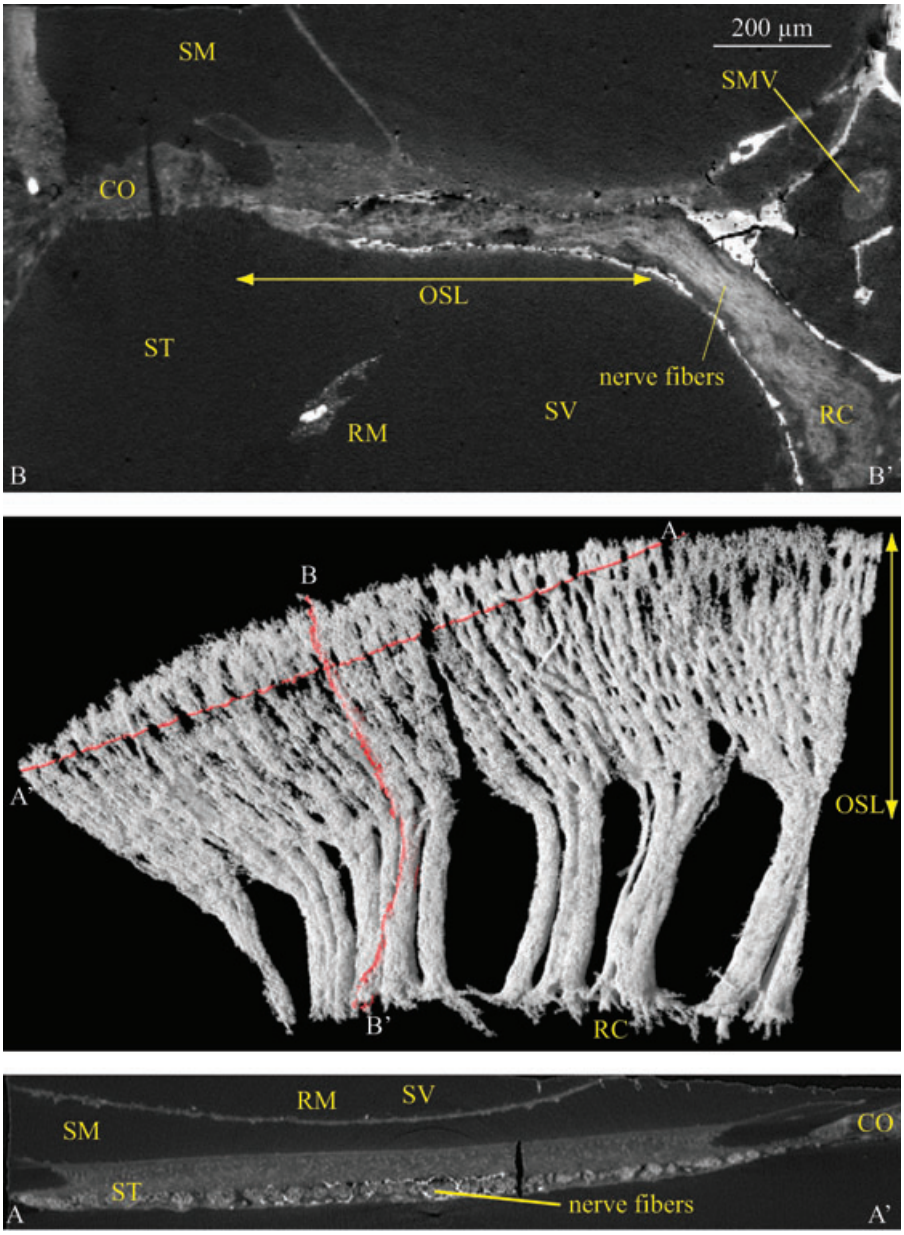


**Fig. 3.** Based on individual 2D slices (images on top and bottom), it is rather difficult to identify the complicated 3D course of the nerve fibre bundles in the human cochlea. For clearness, the morphological features are labeled: Reissner's membrane – RM, osseus spiral lamina – OSL, Rosenthal's canal – RC, spiral modiolar vein – SMV, scala media – SM, scala vestibuli – SV, scala tympani – ST, the nerve fibres in the OSL and the organ of corti – OC. The semi-automatic, intensity-based segmentation of the nerve fibres as given in the middle shows the spatial distribution of the fibre bundles. The orientation of the slices is indicated by red colour in the 3D image and by A-A′ and B-B′ in the slices.

beamline Tomcat using the photon energy of 12 keV. As illuminated by means of a selected tomography slice, the nerve fibre bundles reach from the Rosenthal's canal via the OSL, housing the spiral ganglion neurons, to the sensory epithelium. The wealth of details demonstrates the superior spatial resolution of the tomography data with respect to previous measurements (Vogel, 1999). The 3D representation in the middle of Fig. 3 has been obtained segmenting higher absorbing species in the 2-fold binned tomography data semi-automatically. Although different cell types in the organ of Corti cannot be distinguished, the tunnel of Corti, a fluid-filled space in the sensory epithelium, is clearly visible. The course of the peripheral nerve fibre bundles can be followed from the perikarya in Rosenthal's canal as far as the distal end of the OSL.

The nerve fibres, connected namely to the inner (90–95%) and outer hair cells (5–10%) (Spoendlin, 1985) passing out between the two layers of the lamina spiralis ossea accumulate

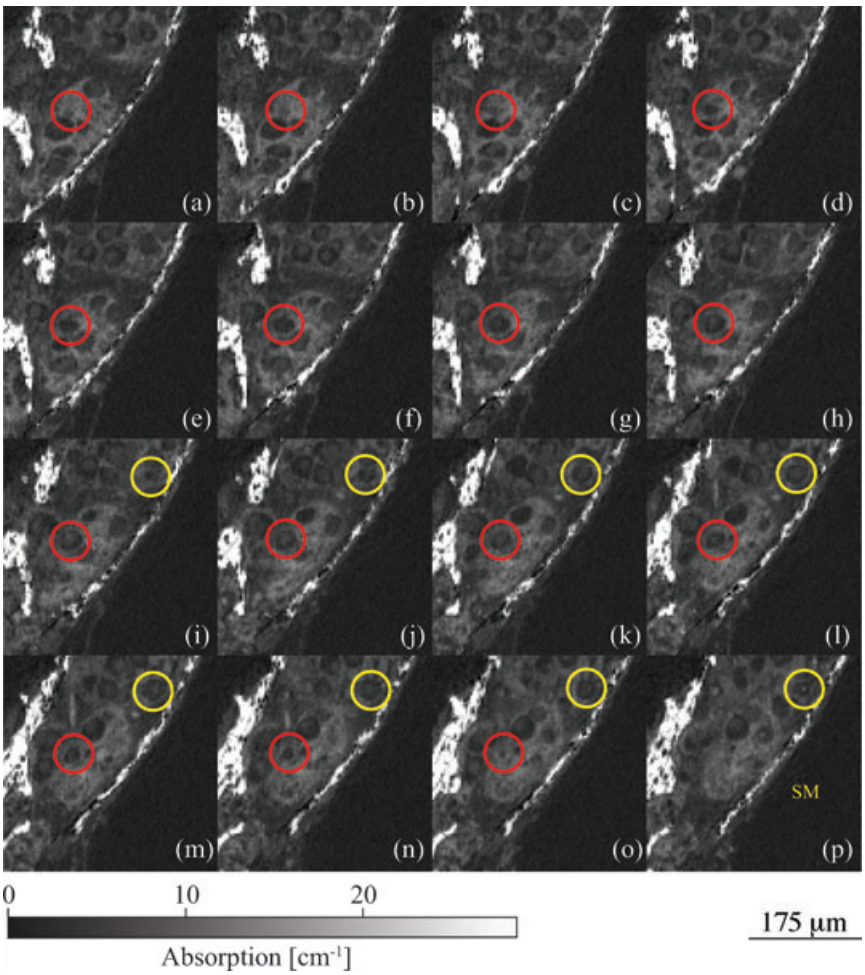


**Fig. 4.** The counting of the individual ganglion cells can be performed manually analyzing subsequent slices of the tomogram. It is exemplarily shown labeling two cells by means of differently coloured circles in 16 slices each 3.5 µm thick.

to bundles en route to the modiolus, the conically shaped central axis in the cochlea. Myelinated nerve fibres are part of bipolar ganglion cells, which send their central projections to the brain stem and form the cochlear nerve (see Fig. 3). The data may provide the basis for the analysis of the complex bifurcation network in the 3D space of the OSL.

The data in Fig. 4, measured at the beamline Tomcat, show a part of the spiral canal, which contains the ganglion cells. The sequence of slices reveals the spherical shape of the ganglion cells, which exhibit diameters of about 30 µm. The counting of 148 clearly identified individual ganglion cells within a volume of 0.125 mm × 0.8 mm × 0.6 mm = 0.06 $mm^3$ corresponds to values given in the literature (Pollak *et al.*, 1987). These values allow estimating the presence of 2000 cells along 1 mm organ of Corti within the analyzed segment. It seems to be important that each ganglion cells consists of a higher absorbing microstructure in the centre of a less absorbing spherical shell that simplifies the cell identification. Figure 5 displays frontal, sagittal and axial views of one dedicated cell in the centre of each slice. These slices point out the spherical shape of the ganglion cells with higher X-ray absorbing central part.

## Discussion

Multi-slice computed tomography (Marincek *et al.*, 2001) and magnetic resonance imaging (Naganawa *et al.*, 1999) belong to the clinical modalities that have achieved a spatial resolution down to the fraction of 1 mm. The cochlea itself has become visible but many anatomical details have been missing (Goldfeld *et al.*, 2005). By means of micro computed tomography (µCT) it has been possible to increase the spatial resolution by two orders of magnitude. U. Vogel (1999) pointed out, however, that the very thin and hollow lamina spiralis ossea has been only imaged weakly, and the membranous labyrinth not at all. In particular, he did not find any indication for the basilar membrane and the organ of Corti despite the spatial resolution was in the 10-µm range.

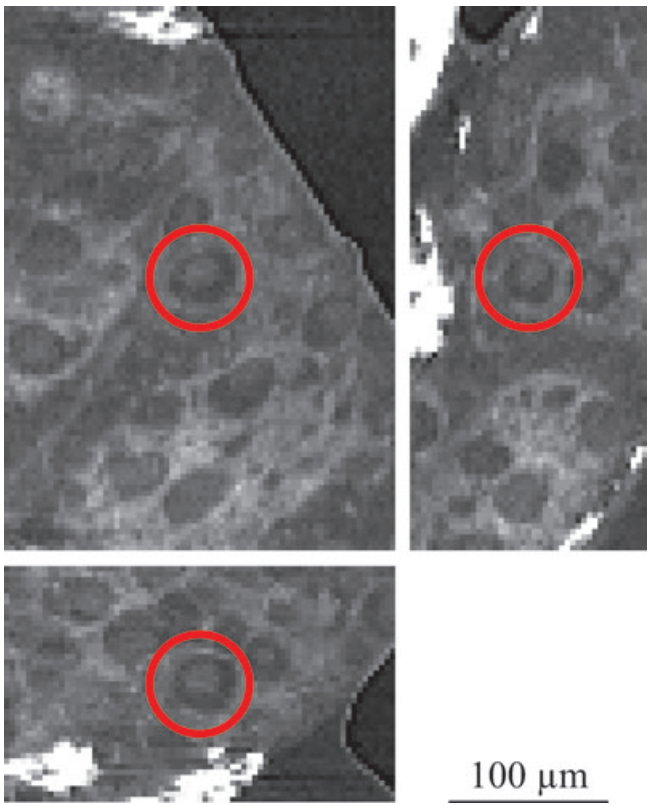


**Fig. 5.** The shape and size of selected ganglion cells can be made visible basically by the frontal, sagittal and axial views. The three slices perpendicular to each another virtually cut the ganglion cell in the centre of each image. The ganglion cells about 30 μm in diameter appear as higher X-ray absorbing feature surrounded by a lower absorbing spherical shell.

T. Shibaba and T. Nagano (1996), who also performed high-resolution microfocus computed tomography of the human auditory apparatus, do not show any cellular feature. The membranes are not mentioned in their manuscript, and from the images one can only estimate that the membranes are somehow thinner than 0.1 mm, maybe about 50 μm. A more recent μCT study (Rau *et al.*, 2006) using coherent synchrotron radiation has shown that the membranes could be made visible because of the edge enhancement, that is, a kind of phase-contrast imaging. This approach allows extracting the 3D shape of the features including membranes. Their segmentation and the representation of the exact thickness are very complex and require other methods for calibration.

The present approach of the membrane staining allows for example measuring the thickness of the Reissner's membrane with reasonable accuracy that corresponds to 10 ± 2 μm. The osmium staining also permits visualizing the nerve fibre network within the basilar membrane because of Os-enrichment in the myelin sheaths with unrivaled precision. Thus, SRμCT is complementary to classical histology rather than competing, since the different immuno-histochemical staining and *in situ* hybridization techniques yield information about cell functions. Functional cell staining procedures for SRμCT experiments yield only restricted information and are, therefore, rare (Müller *et al.*, 2006).

Fundamental limitations of histology are the loss of the sub-micrometre resolution in the third dimension and the occurrence of preparation artefacts such as tissue compression after decalcification and relaxed membranes because of sectioning with the microtom (Martín-Badosa *et al.*, 2003). Stacking the slices to a 3D data set often provides promising results (Li *et al.*, 2006). Nevertheless, preparation artefacts cannot be compensated, and the effort is tremendous. Consequently, the spatial resolution remains restricted to values of about 20 μm (Li *et al.*, 2006; Wang *et al.*, 2006), which is more than one order of magnitude less precise than reached in the present study.

P. Thurner et al. (2003) showed that after appropriate staining, individual human cells of soft tissue, namely, foreskin fibroblasts could be made visible by means of SRμCT. The study, however, was restricted to *in vitro* cell cultures on polymer filaments. To the best of the author's knowledge, the present communication demonstrates for the first time that SRμCT offers the visualization of individual cells in human soft tissue. The acquired high-quality 3D data not only permit the counting of the ganglion cells and the precise determination of their relative location but even show features of the internal cell microstructure with equidistant micrometre resolution. This should lead to a deeper insight of the distribution of neural elements in the cochlea of normal hearing and hearing impaired subjects, important for understanding hearing loss and improving cochlear implants.

## Conclusions

High-resolution tomography of an osmium-stained inner ear using monochromatic X rays offers isotropic sub-cellular spatial resolution and provided the contrast necessary to visualize the morphology of the membranous sensory components, of nerve fibre bundles and of hundreds of individual ganglion cells, non-destructively. Therefore, the present communication demonstrates, for the first time, that X-ray tomography allows visualizing individual cells within human tissue. Individual ganglion cells have been counted and measured in size and shape, although they were encapsulated in highly X-ray absorbing bony tissue, without any sectioning and related artefact occurrence. The preferred accumulation of osmium in the myelin sheaths allows segmenting the nerve fibre bundles, to analyze their splitting and to pursuit the run through the osseus spiral lamina. The intent of the present study was the better understanding of the complex inner ear morphology on the micrometre scale. In fact, the extracted shapes and thicknesses of the membranous sensory microstructures can be used

for educational purposes and provides an important basis for the direct comparison of healthy and altered inner ear morphologies such as dysplastic malformations down to the cellular level and even below.

## Acknowledgement

The experiments were carried out in the frame of the approved proposals 20060267 (SLS at PSI) and I-04-077 (HASYLAB at DESY). We gratefully thank for the excellent support at the beamlines W2 at HASYLAB at DESY, Hamburg, Germany (J. Herzen, T. Donath) and Tomcat at SLS at PSI, Villigen, Switzerland (M. Stampanoni, A. Groso). Furthermore, we thank F. Fierz (University of Basel) for continuous assistance.

## References

Beckmann, F. (2001) Microtomography using synchrotron radiation as a user experiment at beamlines BW2 and BW5 of HASYLAB at DESY. *Developments in X-Ray Tomography III* (ed. by U. Bonse). *Proc. SPIE* **4503**, 34–41.

de Fraissinette, A., Felix, A., Hoffmann, V., Johansson, L.-G. & Gleeson, M.J. (1993) Human Reissner's membrane in patients with age-related normal hearing and with sensorineural hearing loss. *J. Otorhinolaryngol. Relat. Spec.* **55**, 68–72.

Glauert, A.M. (1980) *Fixation, Dehydration and Embedding of Biological Specimens*. North Holland Publishing Company, Amsterdam, New York, Oxford.

Goldfeld, M., Glaser, B., Nassir, E., Gomori, J. M., Hazani, E. & Bishara, N. (2005) CT of the ear in Pendred syndrome. *Radiology* **235**, 537–540.

Kak, A.C. & Slaney, M. (1988) *Principles of Computerized Tomographic Imaging*. IEEE Press, New York.

Kiernan, A.E. (2006) The paintfill method as a tool for analyzing the three-dimensional structure of the inner ear. *Brain Res.* **1091**, 270–276.

Li, S.F., Zhang, T.Y. & Wang, Z.M. (2006) An approach for precise three-dimensional modeling of the human inner ear. *J. Otorhinolaryngol. Relat. Spec.* **68**, 302–310.

Marincek, B., Ros, P.R., Reiser, M. & Baker, M.E. (Eds.) (2001) *Multislice CT: A Practical Guide*. Springer, Berlin, Heidelberg, New York.

Martín-Badosa, E., Amblard, D., Nuzzo, S., Elmoutaouakkil, A., Vico, L. & Peyrin, F. (2003) Excised bone structures in mice: imaging at three-dimensional synchrotron radiation micro CT. *Radiology* **229**, 921–928.

Müller, B., Bernhardt, R., Weitkamp, T., *et al.* (2007) Morphology of bony tissues and implants uncovered by high-resolution tomographic imaging. *Int. J. Mater. Res.* **98**, 613–621.

Müller, B., Riedel, M. & Thurner, P.J. (2006) Three-dimensional characterization of cell clusters using synchrotron-radiation-based micro computed tomography. *Microsc. Microanal.* **12**, 97–105.

Müller, B., Thurner, P., Beckmann, F., *et al.* (2001) Non-destructive three-dimensional evaluation of biocompatible materials by microtomography using synchrotron radiation. *Developments in X-Ray Tomography III* (ed. by U. Bonse). *Proc. SPIE* **4503**, 178–188.

Naganawa, S., Ito, T., Iwayama, E., Fukatsu, H., Ishigaki, T., Nakashima, T. & Ichinose, N. (1999) MR imaging of the cochlear modiolus: area measurement in healthy subjects and in patients with a large endolymphatic duct and sac. *Radiology* **213**, 819–823.

Plouraboué, F., Cloetens, P., Fonta, C., Steyer, A., Lauwers, F. & Marc-Vergnes, J.-P. (2004) X-ray high-resolution vascular network imaging. *J. Microsc.* **215**, 139–148.

Pollak, A., Felix, H. & Schrott, A. (1987) Methodological aspects of quantitative study of siral ganglion cells. *Acta Otolaryngol.* **436**, 37–42.

Rau, C., Robinson, I.K. & Richter, C.P. (2006) Visualizing soft tissue in the mammalian cochlea with coherent hard X-rays. *Microsc. Res. Tech.* **69**, 660–665.

Shibata, T. & Nagano, T. (1996) Applying very high resolution microfocus X-ray CT and 3-D reconstruction to the human auditory apparatus. *Nat. Med.* **2**, 933–935.

Spoendlin, H. & Schrott, A. (1988) The spiral ganglion and the innervation of the human organ of Corti. *Acta Otolaryngol.* **105**, 403–410

Spoendlin, H. & Schrott, A. (1989) Analysis of the human auditory nerve. *Hear Res.* **43**, 25–38.

Spoendlin, M.D. (1985) Anatomy of cochlear innervation. *Am. J. Otolaryngol.* **6**, 453–467.

Stampanoni, M., Groso, A., Isenegger, A., et al. (2006) Trends in synchrotron-based tomographic imaging: the SLS experience. *Developments in X-Ray Tomography V* (ed. by U. Bonse). *Proc. SPIE* **6318**, 63180M.

Thurner, P., Beckmann, F. & Müller, B. (2004) An optimization procedure for spatial and density resolution in hard X-ray micro-computed tomography. *Nucl. Instrum. Meth. B* **225**, 599–603.

Thurner, P., Müller, B., Beckmann, F., *et al.* (2003) Tomography studies of human foreskin fibroblasts on polymer yarns. *Nucl. Instrum. Methods Res. B* **200**, 397–405.

Vogel, U. (1999) New approach for 3D imaging and geometry modelling of the human inner ear. *J. Otorhinolaryngol. Relat. Spec.* **61**, 259–267.

Wang, H., Northrop, C., Burgess, B., Liberman, M.C. & Merchant, S.N. (2006) Three-dimensional virtual model of the human temporal bone: a stand-alone, downloadable teaching tool. *Otol. Neurotol.* **27**, 452–457.